Dressed-state engineering for continuous detection of itinerant microwave photons

Kazuki Koshino,[1] Zhirong Lin,[2] Kunihiro Inomata,[2] Tsuyoshi Yamamoto,[3] and Yasunobu Nakamura[2,4]
[1]*College of Liberal Arts and Sciences, Tokyo Medical and Dental University, Ichikawa, Chiba 272-0827, Japan*
[2]*RIKEN Center for Emergent Matter Science (CEMS), 2-1 Hirosawa, Wako, Saitama 351-0198, Japan*
[3]*Smart Energy Research Laboratories, NEC Corporation, Tsukuba, Ibaraki 305-8501, Japan*
[4]*Research Center for Advanced Science and Technology (RCAST), The University of Tokyo, Meguro-ku, Tokyo 153-8904, Japan*
(Received 14 September 2015; published 18 February 2016)

We propose a scheme for continuous detection of itinerant microwave photons in circuit quantum electrodynamics. In the proposed device, a superconducting qubit is coupled dispersively to two resonators: one is used to form an impedance-matched Λ system that deterministically captures incoming photons, and the other is used for continuous monitoring of the event. The present scheme enables efficient photon detection: for realistic system parameters, the detection efficiency reaches 0.9 with a bandwidth of about 10 MHz.

DOI: 10.1103/PhysRevA.93.023824

I. INTRODUCTION

Microwave quantum optics using superconducting qubits and transmission lines, which is realized in circuit-quantum-electrodynamics setups, is one of the hottest research areas in modern quantum physics [1]. Exploiting the large dipole moment of superconducting qubits, circuit QED enables various quantum-optical phenomena that have not been reached by quantum optics in the visible domain. In particular, we can readily construct optical setups with excellent one-dimensionality [2–4], which are suitable for constructing a scalable quantum circuit. However, the lack of an efficient detector for itinerant microwave photons has been a long-standing problem, and several approaches have been proposed to date. One approach is to capture a propagating photon deterministically into a resonator mode and detect it afterward. In recent experiments, the possibility of such capturing has been demonstrated with an excellent fidelity [5,6]. However, this approach requires precise temporal control of the system parameters that depends on the exact pulse shapes of the signal photons. Another approach is to use the Kerr effect mediated by superconducting qubits [7–9], which may enable nondestructive photon detection. However, it has been revealed that a high distinguishability of the signal photon number can be achieved only by cascading several identical qubits with negligible photon loss in between, which is a challenging technical task presently [8,9]. Recently, microwave photon detectors using the optomechanical systems have been proposed [10,11].

An alternative approach is to use the deterministic switching of a Λ system induced by individual photons [12–14], which has been experimentally realized in one-dimensional systems [15,16]. Note that this occurs as a result of single-photon dynamics: The destructive interference between the input and the elastically scattered photons enables the deterministic operation. Recently, detection of propagating microwave photons has been demonstrated using a Λ system realized in a tilted washboard potential of a current-biased Josephson junction [17–19]. A problem with this scheme could be the substantial dissipation upon detection and the resultant long dead time before resetting. More recently, we realized a Λ system formed by the dressed states of a qubit-resonator system and discussed its performance as a photon detector [14,15,20]. This detector attains a high detection efficiency within the detection bandwidth, regardless of the signal pulse profile and with negligible dark counts. However, this detector should be operated in the time-gated mode, since the drive field to generate the Λ-type transition must be turned off during the qubit readout to obtain a high fidelity.

In this study, we present a practical scheme for continuous detection of itinerant microwave photons. We couple two resonators to a qubit: One is used for forming a Λ system [14,15] and the other is used for continuous qubit monitoring [21–24]. The proposed device enables continuous operation of the photon detector, preserving the advantages of our previous scheme [20], such as a high detection efficiency, insensitivity to the signal pulse shape, and short dead times after detection. Moreover, the efficient detection is possible without cascading qubits [8,9].

II. SYSTEM

We consider a device in which a superconducting qubit is coupled to two resonators A and B (Fig. 1). When setting $\hbar = 1$, this system is described by

$$\mathcal{H}_{\rm sys} = \bar{\omega}_a a^\dagger a + \bar{\omega}_b b^\dagger b + \bar{\omega}_q \sigma^\dagger \sigma + g_a(a^\dagger + a)(\sigma^\dagger + \sigma) + g_b(b^\dagger + b)(\sigma^\dagger + \sigma), \quad (1)$$

where a, b, and σ respectively denote the annihilation operators for resonators A, B, and the qubit. $\bar{\omega}_a$, $\bar{\omega}_b$, and $\bar{\omega}_q$ are their bare frequencies, and g_a and g_b are the qubit-resonator couplings. We consider a case in which the qubit is coupled to two resonators dispersively, namely, $|\bar{\omega}_r - \bar{\omega}_q| \gg g_r$ ($r = a,b$). Then, up to the second-order perturbation in g_r, we can rewrite $\mathcal{H}_{\rm sys}$ into the following diagonal form:

$$\mathcal{H}_{\rm sys} = (\omega_a a^\dagger a + \omega_b b^\dagger b)\sigma\sigma^\dagger + [\omega_q + (\omega_a - 2\chi_a)a^\dagger a + (\omega_b - 2\chi_b)b^\dagger b]\sigma^\dagger\sigma, \quad (2)$$

where $\chi_r = g_r^2/(\bar{\omega}_r - \bar{\omega}_q) - g_r^2/(\bar{\omega}_r + \bar{\omega}_q)$ is called the dispersive shift ($r = a,b$), and the renormalized frequencies of the resonators and the qubit are $\omega_a = \bar{\omega}_a + \chi_a$, $\omega_b = \bar{\omega}_b + \chi_b$, and $\omega_q = \bar{\omega}_q - \chi_a - \chi_b$ [25]. In the following, we set $(\omega_a,\omega_b,\omega_q)/2\pi = (10,12,5)$ GHz and $(\chi_a,\chi_b)/2\pi = (50,20)$ MHz for concreteness.

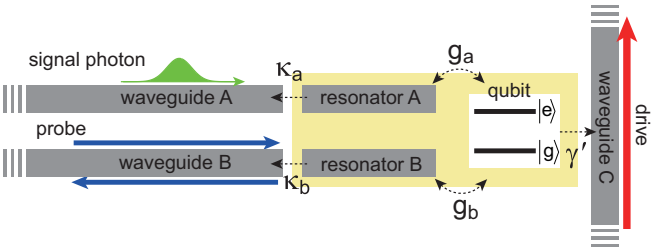

FIG. 1. Schematic of the single-photon detector. A qubit is coupled dispersively to two resonators. Resonators A and B and the qubit are respectively coupled to waveguides A, B, and C. We input a signal photon through waveguide A, a probe field through waveguide B, and a drive field through waveguide C.

The qubit and the resonators are respectively coupled to waveguides, through which we apply three kinds of microwaves (Fig. 1). Through waveguide C, we apply a continuous drive field to the qubit to generate a so-called impedance-matched Λ system by the dressed states of the qubit and resonator A. Through waveguide A, we input a signal photon to be detected, which deterministically induces a Raman transition and excites the qubit. Through waveguide B, we apply a continuous probe field for the dispersive readout of the qubit state.

We denote the radiative decay rates of resonators A and B and the qubit by κ_a, κ_b, and γ', respectively. κ_a determines the bandwidth of the photon detector, which should be smaller than or comparable to the level separation of the dressed states [$|\widetilde{3}\rangle$ and $|\widetilde{4}\rangle$ of Fig. 2(b)]. κ_b determines the phase shift of the probe field upon reflection and $\kappa_b \simeq 2\chi_b$ is favorable for qubit readout [26]. We set $(\kappa_a,\kappa_b)/2\pi = (20,40)$ MHz. Additionally, the qubit undergoes nonradiative decay and its overall decay rate γ often dominates γ'. The photon detection efficiency is sensitive to γ. We assume a reasonably long-lived qubit of $\gamma/2\pi = 0.01$ MHz ($T_1 \approx 16\,\mu$s) [27,28].

III. DRESSED-STATE ENGINEERING

We engineer the dressed states of the qubit-resonators system through the qubit drive. Theoretically, the qubit drive is described by $\mathcal{H}_{dr}(t) = \sqrt{\gamma'}[E_d(t)\sigma^\dagger + E_d^*(t)\sigma]$, where $E_d(t) = E_d e^{-i\omega_d t}$ is a monochromatic drive field. In the frame rotating at ω_d, we obtain a static Hamiltonian,

$$\begin{aligned}\mathcal{H}_{sys+dr} &= (\omega_a a^\dagger a + \omega_b b^\dagger b)\sigma\sigma^\dagger + [(\omega_q - \omega_d) \\ &\quad +(\omega_a - 2\chi_a)a^\dagger a + (\omega_b - 2\chi_b)b^\dagger b]\sigma^\dagger\sigma \\ &\quad +\Omega_d(\sigma^\dagger + \sigma), \end{aligned} \tag{3}$$

where $\Omega_d = \sqrt{\gamma'}E_d$ is the Rabi frequency of the qubit drive. Hereafter, Ω_d represents the drive power.

First, we consider the case with $\Omega_d = 0$. The eigenstates of $\mathcal{H}_{sys+dr}$ are the Fock states $|q,n_a,n_b\rangle$, where $q(= g,e)$ denotes the qubit state and n_a and $n_b(= 0,1,\dots)$ denote the resonator photon numbers. To find the optimal drive conditions, we restrict ourselves to the zero- and one-photon states [Fig. 2(a)]. In this study, we use resonator A to form a Λ system and resonator B as a readout resonator that preserves the qubit state upon transitions. For this purpose, we should realize the level structure of Fig. 2(a),

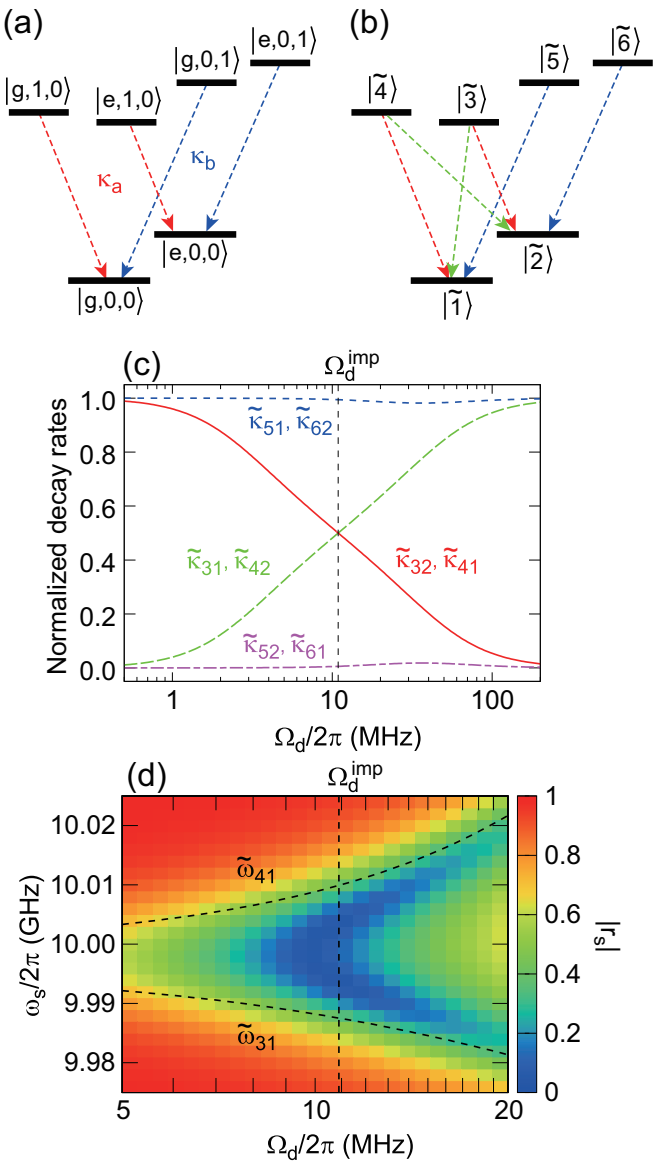

FIG. 2. Dressed-state engineering of the qubit-resonators system. (a) Level structure of the bare states ($\Omega_d = 0$) in the rotating frame. (b) Level structure of the dressed states at the operation point ($\Omega_d = \Omega_d^{imp}$). (c) Dependences of the decay rates on the drive power. The drive frequency is set at $\omega_d/2\pi = 4.905$ GHz. An impedance-matched Λ system is formed at $\Omega_d^{imp}/2\pi = 10.897$ MHz. $\widetilde{\kappa}_{ji}^a$ ($\widetilde{\kappa}_{ji}^b$) is normalized by κ_a (κ_b). (d) Amplitude of the reflection coefficient $|r_s|$ of a continuous signal field applied through waveguide A, as a function of the signal frequency ω_s and the drive power Ω_d. The upper (lower) curve represents $\widetilde{\omega}_{41}$ ($\widetilde{\omega}_{31}$).

where $\omega_{|g,0,0\rangle} < \omega_{|e,0,0\rangle} < \omega_{|e,1,0\rangle} < \omega_{|g,1,0\rangle}$ (nesting regime for resonator A) and $\omega_{|g,0,0\rangle} < \omega_{|e,0,0\rangle} < \omega_{|g,0,1\rangle} < \omega_{|e,0,1\rangle}$ (unnesting regime for resonator B) [14]. This is done by setting the drive frequency within the range of $\omega_q - 2\chi_a < \omega_d < \omega_q - 2\chi_b$.

Next, we consider the case with $\Omega_d > 0$. The drive field mixes the bare states to form the dressed states. We denote the dressed states by $|\widetilde{1}\rangle, |\widetilde{2}\rangle, \dots$ and label them from the lowest

in energy [Fig. 2(b)]. From Eq. (3), they are given by

$$|\widetilde{1}\rangle = \cos\theta_{12}|g,0,0\rangle - \sin\theta_{12}|e,0,0\rangle, \quad (4)$$

$$|\widetilde{2}\rangle = \sin\theta_{12}|g,0,0\rangle + \cos\theta_{12}|e,0,0\rangle, \quad (5)$$

$$|\widetilde{3}\rangle = \cos\theta_{34}|e,1,0\rangle - \sin\theta_{34}|g,1,0\rangle, \quad (6)$$

$$|\widetilde{4}\rangle = \sin\theta_{34}|e,1,0\rangle + \cos\theta_{34}|g,1,0\rangle, \quad (7)$$

$$|\widetilde{5}\rangle = \cos\theta_{56}|g,0,1\rangle - \sin\theta_{56}|e,0,1\rangle, \quad (8)$$

$$|\widetilde{6}\rangle = \sin\theta_{56}|g,0,1\rangle + \cos\theta_{56}|e,0,1\rangle, \quad (9)$$

$$\theta_{12} = \arctan[2\Omega_d/(\omega_{|e,0,0\rangle} - \omega_{|g,0,0\rangle})]/2, \quad (10)$$

$$\theta_{34} = \arctan[2\Omega_d/(\omega_{|g,1,0\rangle} - \omega_{|e,1,0\rangle})]/2, \quad (11)$$

$$\theta_{56} = \arctan[2\Omega_d/(\omega_{|e,0,1\rangle} - \omega_{|g,0,1\rangle})]/2. \quad (12)$$

The radiative decay rate from $|\widetilde{j}\rangle$ ($j = 3,4$) to $|\widetilde{i}\rangle$ ($i = 1,2$) is given by $\widetilde{\kappa}^a_{ji} = \kappa_a|\langle\widetilde{j}|a^\dagger|\widetilde{i}\rangle|^2$. We confirm that $\widetilde{\kappa}^a_{31} = \widetilde{\kappa}^a_{42}$, $\widetilde{\kappa}^a_{32} = \widetilde{\kappa}^a_{41}$, and $\widetilde{\kappa}^a_{31} + \widetilde{\kappa}^a_{32} = \widetilde{\kappa}^a_{41} + \widetilde{\kappa}^a_{42} = \kappa_a$. Namely, $|\widetilde{3}\rangle$ and $|\widetilde{4}\rangle$ decay in two directions, satisfying the sum rule of decay rates. Similarly, $\widetilde{\kappa}^b_{51} = \widetilde{\kappa}^b_{62}$, $\widetilde{\kappa}^b_{52} = \widetilde{\kappa}^b_{61}$, and $\widetilde{\kappa}^b_{51} + \widetilde{\kappa}^b_{52} = \widetilde{\kappa}^b_{61} + \widetilde{\kappa}^b_{62} = \kappa_b$. Figure 2(c) plots $\widetilde{\kappa}^a_{ji}$ and $\widetilde{\kappa}^b_{ji}$ as functions of the drive power. In the drive-off case ($\Omega_d = 0$), $\widetilde{\kappa}^a_{32} = \widetilde{\kappa}^a_{41} = \kappa_a$, $\widetilde{\kappa}^b_{51} = \widetilde{\kappa}^b_{62} = \kappa_b$, and others vanish. This represents the simple decay of the resonator modes preserving the qubit state [Fig. 2(a)]. As we increase the drive power, the decay rates for resonator A are inverted, whereas those for resonator B remain almost unchanged. This is because of our choice of the drive frequency ω_d. At $\Omega_d^{\rm imp}$ in Fig. 2(c), the four decay rates concerning resonator A become identical. Then, a resonant signal photon deterministically induces a Raman transition of $|\widetilde{1}\rangle \to |\widetilde{j}\rangle \to |\widetilde{2}\rangle$ ($j = 3,4$). Regarding resonator B, we should make $\widetilde{\kappa}^b_{52}(= \widetilde{\kappa}^b_{61})$ as small as possible to suppress the $|\widetilde{1}\rangle \to |\widetilde{k}\rangle \to |\widetilde{2}\rangle$ and $|\widetilde{2}\rangle \to |\widetilde{k}\rangle \to |\widetilde{1}\rangle$ transitions ($k = 5,6$). For this purpose, ω_d close to $\omega_q - 2\chi_a$ is advantageous. We set $\omega_d/2\pi = 4.905$ GHz [5 MHz above $(\omega_q - 2\chi_a)/2\pi$] hereafter, which results in $\Omega_d^{\rm imp}/2\pi = 10.897$ MHz. Then, $\cos^2\theta_{12} = 0.99$, $\cos^2\theta_{34} = 0.61$, and $\cos^2\theta_{56} = 0.96$. Namely, the dressed states $|\widetilde{1}\rangle$, $|\widetilde{2}\rangle$, $|\widetilde{5}\rangle$, and $|\widetilde{6}\rangle$ are almost identical to the bare states $|g,0,0\rangle$, $|e,0,0\rangle$, $|g,0,1\rangle$, and $|e,0,1\rangle$, respectively. $\widetilde{\kappa}^b_{52}(= \widetilde{\kappa}^b_{61})$ is about 0.6% of κ_b.

IV. SNR AND DETECTION EFFICIENCY

In the proposed detector, a signal photon is expected to excite the qubit with a high probability. In order to continuously monitor this event, we apply a probe field, $E_p(t) = E_p e^{-i\omega_p t}$, through waveguide B [21–24]. From Eq. (2), the resonant frequency of resonator B depends on the qubit state. This is reflected in the phase shift of the probe field upon reflection. The phase shift θ_g for the qubit ground state is given by $\theta_g = 2\arctan[\kappa_b/2(\omega_b - \omega_p)]$, and θ_e for the qubit excited state is obtained by replacing ω_b with $\omega_b - 2\chi_b$. Hereafter, in order to suppress the $|\widetilde{1}\rangle \to |\widetilde{5}\rangle$ transition, we set the probe frequency at $\omega_p = \omega_b - 2\chi_b$ rather than the usually chosen condition $\omega_p = \omega_b - \chi_b$. This results in $e^{i\theta_g} = (3 + 4i)/5$ and $e^{i\theta_e} = -1$. We measure one quadrature of the reflected field for discriminating the qubit state. We infer the qubit state through the time-averaged probe field with an integration time Δt. The signal-to-noise ratio (SNR) is given, assuming that the noise is purely of quantum origin, by

$$\mathrm{SNR} = \sqrt{\frac{\kappa_b\langle n_b\rangle\Delta t}{4}}\left|e^{i\theta_g} - e^{i\theta_e}\right|, \quad (13)$$

where $\langle n_b\rangle = 4|E_p|^2/\kappa_b$ represents the probe power in terms of the mean photon number in resonator B [21]. The readout fidelity $\mathcal{F}$ is given by

$$\mathcal{F} = \mathrm{erf}(\mathrm{SNR}/\sqrt{2}), \quad (14)$$

where erf denotes the error function [29]. In practice, the noise could be enhanced by technical reasons such as the noise from the amplifiers. Here, we assume the noiseless phase-sensitive amplification preserving the SNR [30].

The single-photon detection efficiency η, which is the probability to find the qubit excitation, is evaluated as follows. We denote the qubit excitation probability by $p_e(t)$. Since we infer the qubit state through the time-averaged amplitude, we introduce the time-averaged excitation probability,

$$\overline{p}_e(t) = \frac{1}{\Delta t}\int_{t-\Delta t}^{t} dt'\, p_e(t'), \quad (15)$$

and find the maximum probability $\overline{p}_e(t_m)$ in time. Considering that the probability to correctly infer the qubit state is $(1 + \mathcal{F})/2$, η is given by

$$\eta = \overline{p}_e(t_m)\frac{1+\mathcal{F}}{2} + [1 - \overline{p}_e(t_m)]\frac{1-\mathcal{F}}{2}. \quad (16)$$

$\eta \simeq 1/2$ for a low SNR, implying that the qubit state is completely indistinguishable. In contrast, $\eta \simeq \overline{p}_e(t_m)$ for a high SNR. Note that the detection efficiency is defined in terms of the quantum jumps in actual measurements. In Appendix B, we observe that the present detection efficiency, which is based on the time-averaged qubit excitation probability, is justified by considering the quantum jumps.

V. NUMERICAL RESULTS

In this section, we observe the microwave response of the qubit-resonator system to the signal photon and evaluate the detection efficiency of the detector. The equations of motion used in the numerical simulation are presented in Appendix A.

A. Impedance matching

In the proposed setup, we input a signal photon through waveguide A. Here, in order to find the optimal operating point of the detector, we apply a weak continuous field $E_s(t) = E_s e^{-i\omega_s t}$ through waveguide A and observe its reflection coefficient. The amplitude $|r_s|$ of the reflection coefficient is plotted in Fig. 2(d). We observe that impedance matching ($|r_s| \simeq 0$) takes place at $\Omega_d \simeq \Omega_d^{\rm imp}$ and $\widetilde{\omega}_{31} \lesssim \omega_s \lesssim \widetilde{\omega}_{41}$, where $\widetilde{\omega}_{ji}$ denotes the transition frequency between $|\widetilde{j}\rangle$ and $|\widetilde{i}\rangle$. This indicates that each signal photon induces the Raman transition in the Λ system and is absorbed deterministically.

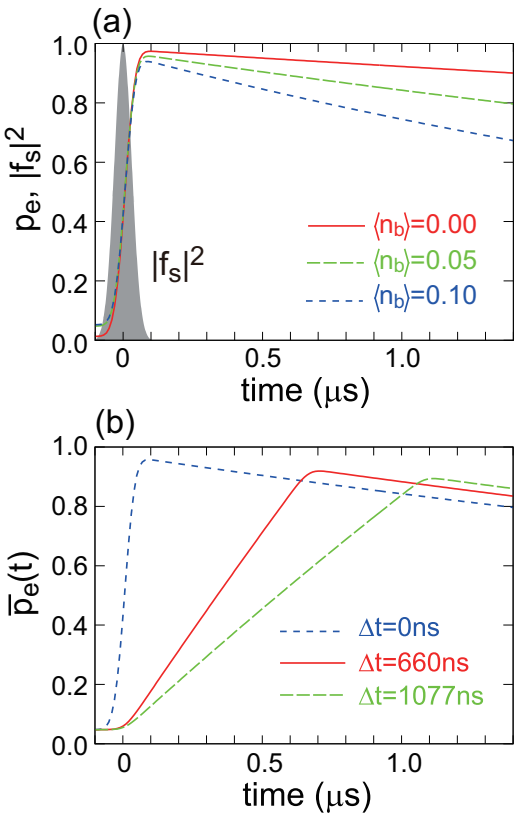

FIG. 3. Microwave response to a signal photon. The signal photon has a carrier frequency of $\omega_s/2\pi = 10.00$ GHz and a Gaussian pulse shape with the length of $l = 100$ ns. (a) Time evolution of the qubit excitation probability $p_e(t)$. The probe power $\langle n_b\rangle$ is indicated. The signal-photon profile $|f_s(t)|^2$ is also shown in units of $(8\ln 2/\pi l^2)^{1/2}$. (b) Time-averaged qubit excitation probability $\overline{p}_e(t)$ for $\langle n_b\rangle = 0.05$. The integration time Δt is indicated.

We choose the drive power and signal frequency as the operating points of the photon detector.

B. Time evolution of qubit excitation probability

We observe the time evolution of the qubit excitation probability $p_e(t)$ induced by a single-photon signal. The signal photon is assumed to be a Gaussian pulse with length l and frequency ω_s, namely,

$$f_s(t) = \left(\frac{8\ln 2}{\pi l^2}\right)^{1/4} 2^{-(2t/l)^2} e^{-i\omega_s t}, \tag{17}$$

which is normalized as $\int dt|f_s(t)|^2 = 1$. Setting $\omega_s/2\pi = 10.00$ GHz and $l = 100$ ns, we plot in Fig. 3(a) the time evolution of the qubit excitation probability $p_e(t)$ for various probe power $\langle n_b\rangle$. First, we observe the case with no probe field [red solid line in Fig. 3(a)]. $p_e(t)$ increases within the pulse duration and approaches to unity, which agrees well with $\int_{-\infty}^{t} dt'|f_s(t')|^2$. A high efficiency is attained regardless of the pulse shape as long as the linewidth of the photon is narrower than that of the Λ system. After the pulse duration, $p_e(t)$ decreases gradually by natural decay of the qubit with rate γ.

We observe that the near-deterministic qubit excitation is degraded by increasing the probe power [green dashed and blue dotted lines in Fig. 3(a)]. This is attributed mainly to the enhanced qubit decay through the $|\widetilde{2}\rangle \to |\widetilde{k}\rangle \to |\widetilde{1}\rangle$ transition ($k = 5,6$). However, for the probe power considered here, the backaction of the qubit readout is not severe and the qubit excitation is maintained for several microseconds. Hereafter, we fix the probe power at $\langle n_b\rangle = 0.05$. Then, $\mathcal{F} = 0.99$ (0.999) [SNR = 2.58 (3.29)] is attained by taking $\Delta t = 660$ (1077) ns. The long qubit lifetime enables us to take such long integration times.

In Fig. 3(b), we plot the time-averaged qubit excitation probability $\overline{p}_e(t)$, which is defined by Eq. (15), for various Δt. Expectedly, $\overline{p}_e(t)$ becomes flatter as we increase Δt, which implies the loss of detection signal. However, owing to the long qubit lifetime, the decrease of $\overline{p}_e(t)$ due to the time-averaging is at most several percent.

C. Detection efficiency

In Fig. 4(a), we plot the efficiency as a function of the pulse length l of the signal photon. If the qubit lifetime is infinite, the efficiency increases monotonically with l. In practice, the efficiency is maximized at a finite pulse length due to the qubit decay during the pulse duration. We observe that a high efficiency is maintained for a wide range of l, which is an advantage of the Λ-based scheme. The loss of efficiency is due to the infidelity of the qubit measurement for short Δt, whereas it is due to the time-averaging for long Δt. For $\Delta t = 660$ ns ($\mathcal{F} = 0.99$), the maximum efficiency of 0.93 is obtained at $l \simeq 100$ ns.

In Fig. 4(b), we plot the efficiency as a function of Ω_d and ω_s. Comparing this with Fig. 2(d), we confirm that the impedance matching leads to a high detection efficiency. The cross section of Fig. 4(b) at $\Omega_d = \Omega_d^{\rm imp}$ is shown in Fig. 4(c) by the red solid line, which shows the detection band of this detector. The detection efficiency exceeds 0.9 (0.8) for a bandwidth of 11 MHz (20 MHz).

D. Discussion

Four final comments are in order. (i) The detector is insensitive to signal photons when the qubit is excited. This causes a dead time of the detector, which amounts to several microseconds at the probe power of $\langle n_b\rangle = 0.05$ [Fig. 3(a)]. However, by applying a reset pulse upon detection of the qubit excitation [20], we may shorten the dead time to several hundreds of nanoseconds. (ii) The detection band center is tunable by changing the drive condition. We show the detection band for different drive conditions in Fig. 4(c). The detection band has two peaks located at $\widetilde{\omega}_{31}$ and $\widetilde{\omega}_{41}$ in general. However, as we increase ω_d and accordingly $\Omega_d^{\rm imp}$, $\widetilde{\kappa}_{52}$, and $\widetilde{\kappa}_{61}$ are increased. This enhances the probe backaction and degrades the detection efficiency. (iii) In the continuous measurement, one may worry that the quantum Zeno effect prohibits efficient photon detection, since the apparent measurement time interval seems infinitely small. However, even in the continuous measurement, the effective measurement time interval Δt_m remains finite, which is determined by the dephasing rate induced by the measuring apparatus [31,32]. Here, the probe field functions as the apparatus and Δt_m is determined by SNR ~ 1, namely, $\Delta t_m \sim 1/\kappa_b\langle n_b\rangle \sim 100$ ns. This is obviously long enough to avoid the Zeno effect

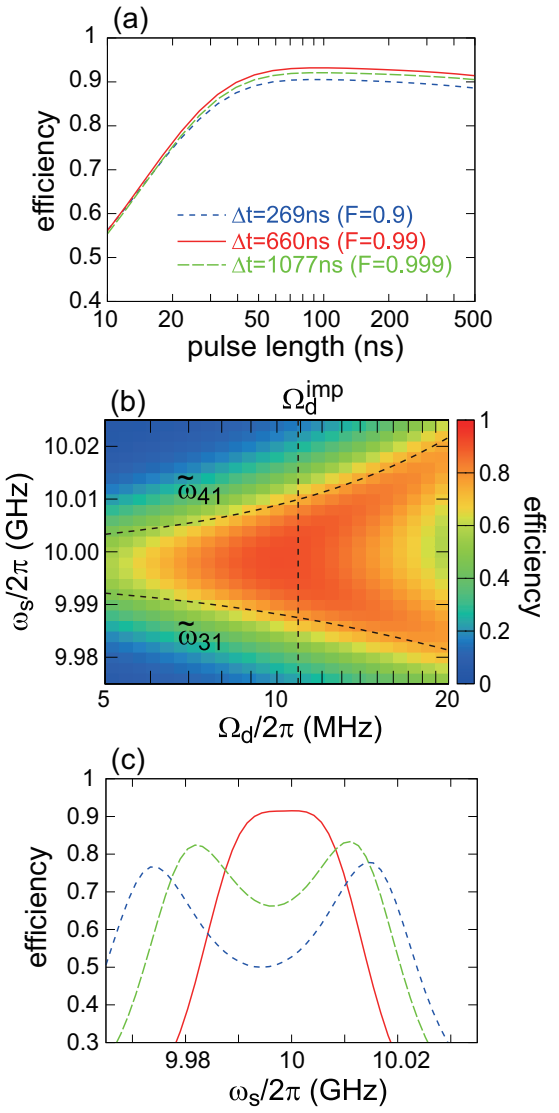

FIG. 4. Single-photon detection efficiency. The probe power is fixed at $\langle n_b \rangle = 0.05$. (a) Dependence of the detection efficiency on the pulse length l for various integration times Δt. Values of the corresponding readout fidelity $\mathcal{F}$ are also indicated. The input photon is tuned at $\omega_s/2\pi = 10.0$ GHz. (b) Detection efficiency as a function of Ω_d and ω_s for $l = 100$ ns and $\Delta t = 660$ ns. The dashed lines indicate $\tilde{\omega}_{41}$, $\tilde{\omega}_{31}$, and $\Omega_d^{\rm imp}$. (c) Cross section of (b) at $\Omega_d^{\rm imp}/2\pi = 10.90$ MHz (red solid). The results for different drive conditions are also shown: $\omega_d/2\pi = 4.913$ GHz and $\Omega_d^{\rm imp}/2\pi = 16.82$ MHz (green dashed) and $\omega_d/2\pi = 4.921$ GHz and $\Omega_d^{\rm imp}/2\pi = 20.37$ MHz (blue dotted).

[see Fig. 3(a)]. (iv) The probe photons may cause the dark counts by inducing the $|\widetilde{1}\rangle \to |\widetilde{k}\rangle \to |\widetilde{2}\rangle$ transition ($k = 5,6$). We can numerically check that this probability is about 0.2% per one probe photon. Therefore, the dark count rate is estimated to be $(142\,\mu{\rm s})^{-1}$ for $\langle n_b \rangle = 0.05$. A lower dark count rate is accomplished by reducing the probe power.

VI. SUMMARY

In summary, we proposed a practical scheme for continuous detection of itinerant microwave photons. The detector consists of a qubit and two resonators in the dispersive regime. We apply a drive field to the qubit to form an impedance-matched Λ system, a signal photon to one of the resonators to excite the qubit, and a probe field to the other to continuously monitor the qubit. For realistic system parameters, the detector has a maximum detection efficiency exceeding 0.9 and a bandwidth of about 10 MHz. One can improve the performance of the detector further by increasing the qubit lifetime and/or the dispersive shifts.

ACKNOWLEDGMENTS

This work was partly supported by JSPS KAKENHI (Grants No. 25400417 and No. 26220601), Project for Developing Innovation Systems of MEXT, National Institute of Information and Communications Technology (NICT), and ImPACT Program of Council for Science, Technology, and Innovation.

APPENDIX A: HEISENBERG EQUATIONS

Here we present the equations of motion for the numerical simulation in Sec. V. The Hamiltonian of the overall system including the three waveguides in Fig. 1 is given by

$$\mathcal{H} = \mathcal{H}_{\rm sys} + \mathcal{H}_{\rm damp}, \tag{A1}$$

$$\mathcal{H}_{\rm sys} = (\omega_a a^\dagger a + \omega_b b^\dagger b)\sigma\sigma^\dagger + [\omega_q + (\omega_a - 2\chi_a)a^\dagger a + (\omega_b - 2\chi_b)b^\dagger b]\sigma^\dagger\sigma, \tag{A2}$$

$$\mathcal{H}_{\rm damp} = \int dk[k a_k^\dagger a_k + \sqrt{\kappa_a/2\pi}(a^\dagger a_k + a_k^\dagger a)] + \int dk[k b_k^\dagger b_k + \sqrt{\kappa_b/2\pi}(b^\dagger b_k + b_k^\dagger b)] + \int dk[k c_k^\dagger c_k + \sqrt{\gamma'/2\pi}(\sigma^\dagger c_k + c_k^\dagger \sigma)], \tag{A3}$$

where a_k, b_k, and c_k respectively denote the annihilation operator propagating in waveguides A, B, and C with wave number k. The term representing the nonradiative decay of the qubit is omitted here. We introduce the real-space representation of a_k by $\widetilde{a}_r = (2\pi)^{-1/2}\int dk e^{ikr} a_k$. In this representation, the $r < 0$ ($r > 0$) region corresponds to the incoming (outgoing) field. From $\mathcal{H}_{\rm damp}$ of Eq. (A3), the following input-output relation is derived:

$$\widetilde{a}_r(t) = \widetilde{a}_{r-t}(0) - i\sqrt{\kappa_a}a(t-r)\theta(r)\theta(t-r). \tag{A4}$$

The input and output field operators are defined at $r = \pm 0$ by $a_{\rm in}(t) = \widetilde{a}_{-0}(t)$ and $a_{\rm out}(t) = \widetilde{a}_{+0}(t)$. $b_{\rm in}(t)$, $b_{\rm out}(t)$, $c_{\rm in}(t)$, and $c_{\rm out}(t)$ are defined similarly. The Heisenberg equation for any system operator S (composed of σ, a, b and their conjugates) is given by

$$\frac{d}{dt}S = i[\mathcal{H}_{\rm sys}, S] + \frac{\kappa_a}{2}(2a^\dagger S a - a^\dagger a S - S a^\dagger a) + \frac{\kappa_b}{2}(2b^\dagger S b - b^\dagger b S - S b^\dagger b) + \frac{\gamma}{2}(2\sigma^\dagger S\sigma - \sigma^\dagger\sigma S - S\sigma^\dagger\sigma)$$

$$+ i\sqrt{\kappa_a}a_{\rm in}^\dagger(t)[a,S] + i\sqrt{\kappa_a}[a^\dagger,S]a_{\rm in}(t)$$
$$+ i\sqrt{\kappa_b}b_{\rm in}^\dagger(t)[b,S] + i\sqrt{\kappa_b}[b^\dagger,S]b_{\rm in}(t)$$
$$+ i\sqrt{\gamma'}c_{\rm in}^\dagger(t)[\sigma,S] + i\sqrt{\gamma'}[\sigma^\dagger,S]c_{\rm in}(t). \quad \text{(A5)}$$

Note that γ is the total decay rate of the qubit including the nonradiative decay.

In our setup, we simultaneously input a single-photon pulse and continuous classical fields. Analysis of the single-photon response is simplified by (i) replacing the single-photon state $|1\rangle$ with a coherent state $|\alpha\rangle$, (ii) performing perturbation calculation with respect to α, and (iii) picking up the relevant terms afterwards [33]. Therefore, we investigate a situation in which a classical pulse $\alpha f_s(t)$ is applied through waveguide A, a probe field $E_p(t)$ is applied through waveguide B, and a drive field $E_d(t)$ is applied through waveguide C. Since classical fields are in the coherent states and are therefore the eigenstates of the input field operators, we may replace the input-field operators with the corresponding field amplitudes. Then, the expectation value of an operator S evolves as

$$\frac{d}{dt}\langle S\rangle_c = i\langle[\mathcal{H}_{\rm sys},S]\rangle_c + \frac{\kappa_a}{2}(2\langle a^\dagger Sa\rangle_c - \langle a^\dagger aS\rangle_c - \langle Sa^\dagger a\rangle_c)$$
$$+ \frac{\kappa_b}{2}(2\langle b^\dagger Sb\rangle_c - \langle b^\dagger bS\rangle_c - \langle Sb^\dagger b\rangle_c)$$
$$+ \frac{\gamma}{2}(2\langle\sigma^\dagger S\sigma\rangle_c - \langle\sigma^\dagger\sigma S\rangle_c - \langle S\sigma^\dagger\sigma\rangle_c)$$
$$+ i\sqrt{\kappa_a}\alpha^* f_s^*(t)\langle[a,S]\rangle_c + i\sqrt{\kappa_a}\langle[a^\dagger,S]\rangle_c\alpha f_s(t)$$
$$+ i\sqrt{\kappa_b}E_p^*(t)\langle[b,S]\rangle_c + i\sqrt{\kappa_b}\langle[b^\dagger,S]\rangle_c E_p(t)$$
$$+ i\sqrt{\gamma'}E_d(t)\langle[\sigma,S]\rangle_c + i\sqrt{\gamma'}\langle[\sigma^\dagger,S]\rangle_c E_d(t). \quad \text{(A6)}$$

We expand $\langle S\rangle_c$ as $\langle S\rangle_c = \sum_{m,n=0}^{\infty}(\alpha^*)^m\alpha^n\langle S\rangle_c^{mn}$. The expectation value $\langle S\rangle_s$ for a single-photon input is obtained by

$$\langle S\rangle_s = \langle S\rangle_c^{00} + \langle S\rangle_c^{11}. \quad \text{(A7)}$$

Note that $\langle S\rangle_c^{00}$ is the stationary solution in the absence of the signal photon. We solve the simultaneous differential equations for $\langle S\rangle_c^{01}$, $\langle S\rangle_c^{10}$, and $\langle S\rangle_c^{11}$ to determine $\langle S\rangle_c^{11}$.

APPENDIX B: DETECTION EFFICIENCY

In the main part of this study, we defined the detection efficiency intuitively through the time-averaged qubit excitation probability. Here, we investigate the detection efficiency more rigorously on the basis of the quantum jumps of the qubit. We observe that the deviation between these two definitions is negligible for the parameter range discussed in this study.

1. Time-independent case

In the dispersive readout of the qubit state, we infer the qubit state through the time-averaged probe field. First, we preliminarily observe a case in which the qubit keeps staying in its ground or excited state. We denote the field operator for the probe port by $c(t)$, which is normalized as $[c(t),c^\dagger(t')] = \delta(t-t')$. We apply a classical field (coherent state) as the probe of the qubit state. The phase of the probe field is sensitive to the qubit state as

$$\langle c(t)\rangle = \begin{cases} E_p e^{i\theta_g} & \text{for } |g\rangle \\ E_p e^{i\theta_e} & \text{for } |e\rangle \end{cases}, \quad \text{(B1)}$$

where the natural phase factor $e^{-i\omega_p t}$ is neglected. We introduce the time-averaged field operator by

$$\bar{c}(t) = \frac{1}{\sqrt{\Delta t}}\int_{t-\Delta t}^{t} dt' c(t'), \quad \text{(B2)}$$

which is normalized as $[\bar{c}(t),\bar{c}^\dagger(t)] = 1$. We infer the qubit state through one of its quadratures, $\bar{x}(t) = {\rm Im}[e^{-i(\theta_g+\theta_e)/2}\bar{c}(t)]$, which maximizes the signal-to-noise ratio (SNR). The expectation value of this operator is

$$\langle\bar{x}(t)\rangle = \begin{cases} -E_p\sqrt{\Delta t}\sin\left(\frac{\theta_e-\theta_g}{2}\right) & \text{for } |g\rangle \\ E_p\sqrt{\Delta t}\sin\left(\frac{\theta_e-\theta_g}{2}\right) & \text{for } |e\rangle \end{cases}. \quad \text{(B3)}$$

We set the threshold at $\langle\bar{x}\rangle = 0$ and judge the qubit state through the sign of $\langle\bar{x}\rangle$. Since $\bar{c}(t)$ is normalized as $[\bar{c}(t),\bar{c}^\dagger(t)] = 1$, the quantum noise in each quadrature is 1/2 for a coherent state. The SNR and the readout fidelity are then given by

$${\rm SNR} = 2E_p\sqrt{\Delta t}\sin\left(\frac{\theta_e-\theta_g}{2}\right), \quad \text{(B4)}$$
$$\mathcal{F} = {\rm erf}({\rm SNR}/\sqrt{2}), \quad \text{(B5)}$$

which are Eqs. (13) and (14) of the main part. The probability to correctly infer the qubit state is $(1+\mathcal{F})/2$.

2. Time-dependent case

Next we investigate a more realistic situation in which the qubit is excited at $t \sim 0$ and decays gradually afterward [Fig. 3(a)]. The detection efficiency η is defined as the probability to detect the qubit excitation. We compare two methods for evaluating this probability: In method 1, which we adopted in the main part of this study, we intuitively evaluate the detection efficiency η_1 through the time-averaged qubit excitation probability. In method 2, we evaluate the detection efficiency η_2 more rigorously based on the quantum jumps of the qubit observed in actual measurements.

a. Method 1

In the main part of this study, we evaluate the detection efficiency as follows. From the qubit excitation probability $p_e(t)$, we define the time-averaged probability $\bar{p}_e(t)$ by

$$\bar{p}_e(t) = \frac{1}{\Delta t}\int_{t-\Delta t}^{t} dt'\, p_e(t'), \quad \text{(B6)}$$

and find the moment t_m that maximizes $\bar{p}_e(t)$. We define the detection efficiency η_1 as the probability to detect the qubit excitation at this moment. Considering that the probability to correctly infer the qubit state is $(1+\mathcal{F})/2$, η_1 is given by

$$\eta_1 = \bar{p}_e(t_m)\frac{1+\mathcal{F}}{2} + [1-\bar{p}_e(t_m)]\frac{1-\mathcal{F}}{2}. \quad \text{(B7)}$$

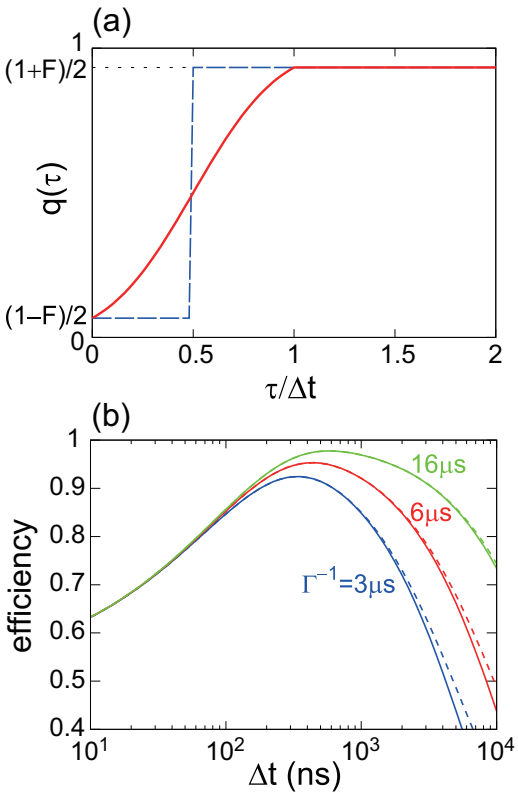

FIG. 5. (a) The probability $q(\tau)$ to detect the qubit excitation as a function of the excitation duration time τ (red solid) and its step-function approximation (blue dashed). (b) Comparison of η_1 (dotted) and η_2 (solid). The qubit lifetime Γ^{-1} is assumed to be 3 μs (blue), 6 μs (red), and 16 μs (green).

b. Method 2

The qubit excitation and de-excitation is observed as the quantum jumps in actual measurements. We consider a single event where the qubit is excited at $t = 0$ and is de-excited at $t = \tau$. Considering the rapid response time of the resonator ($1/\kappa_b \simeq 3.5$ ns), we may regard that the probe field responds immediately to the quantum jumps of the qubit as

$$\langle c(t)\rangle = \begin{cases} E_p e^{i\theta_g} & (t < 0, \tau < t) \\ E_p e^{i\theta_e} & (0 \leqslant t \leqslant \tau) \end{cases}. \tag{B8}$$

$\langle \bar{x}\rangle$ is maximized at $t = (\tau + \Delta t)/2$. The maximum value depends on the duration τ of the qubit excitation as

$$\langle \bar{x}\rangle = \begin{cases} -E_p\sqrt{\Delta t}\sin\left(\frac{\theta_e-\theta_g}{2}\right)\left(1-2\frac{\tau}{\Delta t}\right) & (0 < \tau < \Delta t) \\ E_p\sqrt{\Delta t}\sin\left(\frac{\theta_e-\theta_g}{2}\right) & (\Delta t < \tau) \end{cases}. \tag{B9}$$

Accordingly, the probability $q(\tau)$ to detect the qubit excitation is

$$q(\tau) = \begin{cases} \frac{1}{2}\left\{1-\mathrm{erf}\left[\frac{\mathrm{SNR}}{\sqrt{2}}\left(1-2\frac{\tau}{\Delta t}\right)\right]\right\} & (0 \leqslant \tau \leqslant \Delta t) \\ \frac{1}{2}\left[1+\mathrm{erf}\left(\frac{\mathrm{SNR}}{\sqrt{2}}\right)\right] & (\Delta t < \tau) \end{cases}. \tag{B10}$$

The shape of $q(\tau)$ is shown in Fig. 5(a). It is a monotonically increasing function of τ and becomes constant for $\tau > \Delta t$.

We denote the probability distribution function of the duration τ of the qubit excitation by $Q(\tau)$, which is normalized as $\int_0^\infty d\tau\, Q(\tau) = 1$. Then, the overall probability η_2 to detect the qubit excitation is

$$\eta_2 = \int_0^\infty d\tau\, Q(\tau) q(\tau). \tag{B11}$$

c. Comparison of η_1 and η_2

Here we compare η_1 and η_2 assuming a simple case in which the qubit is excited at $t = 0$ and decays exponentially with a rate of Γ. The excitation probability $p_e(t)$ is given by

$$p_e(t) = \theta(t) e^{-\Gamma t}, \tag{B12}$$

where $\theta(t)$ is the step function. The probability distribution $Q(\tau)$ is connected to $p_e(t)$ by $\int_t^\infty d\tau\, Q(\tau) = p_e(t)$. $Q(\tau)$ is therefore given by

$$Q(\tau) = \Gamma e^{-\Gamma\tau}. \tag{B13}$$

We can show that η_1 and η_2 are almost identical if the qubit decay within the integration time Δt is small, namely, $\Gamma\Delta t \lesssim 1$. Regarding η_1, $\bar{p}_e(t)$ is maximized at $t_m = \Delta t$, and the maximum value $\bar{p}_e(t_m)$ is approximated well by $p_e(\Delta t/2)$. Equation (B7) is then rewritten as

$$\eta_1 = p_e(\Delta t/2)\frac{1+\mathcal{F}}{2} + [1 - p_e(\Delta t/2)]\frac{1-\mathcal{F}}{2}. \tag{B14}$$

On the other hand, regarding η_2, we may replace $q(\tau)$ by a step function [dashed line in Fig. 5(a)] as long as $Q(\tau)$ is almost constant for $0 \leqslant \tau \leqslant \Delta t$. Then, using $\int_{\Delta t/2}^\infty d\tau\, Q(\tau) = p_e(\Delta t/2)$, η_2 is rewritten as

$$\eta_2 = p_e(\Delta t/2)\frac{1+\mathcal{F}}{2} + [1 - p_e(\Delta t/2)]\frac{1-\mathcal{F}}{2}, \tag{B15}$$

which coincides with η_1 of Eq. (B14).

In Fig. 5(b), η_1 and η_2 are plotted as functions of the integration time Δt, setting the probe power at $\langle n_b\rangle = 0.05$. We confirm that the deviation between η_1 and η_2 is small for $\Delta t \lesssim \Gamma^{-1}$. From Fig. 3(a), we estimate that the qubit lifetime is about 6 μs for $\langle n_b\rangle = 0.05$. Then, $|\eta_1 - \eta_2| \lesssim 0.01\%$ for $\Delta t \lesssim 1$ μs. Thus, we can safely regard η_1 as the detection efficiency.

[1] A. Wallraff, D. I. Schuster, A. Blais, L. Frunzio, R. S. Huang, J. Majer, S. Kumar, S. M. Girvin, and R. J. Schoelkopf, Nature (London) **431**, 162 (2004).

[2] O. Astafiev, A. M. Zagoskin, A. A. Abdumalikov, Jr., Yu. A. Pashkin, T. Yamamoto, K. Inomata, Y. Nakamura, and J. S. Tsai, Science **327**, 840 (2010).

[3] I.-C. Hoi, C. M. Wilson, G. Johansson, T. Palomaki, B. Peropadre, and P. Delsing, Phys. Rev. Lett. **107**, 073601 (2011).

[4] A. F. van Loo, A. Fedorov, K. Lalumiere, B. C. Sanders, A. Blais, and A. Wallraff, Science **342**, 1494 (2013).

[5] Y. Yin, Y. Chen, D. Sank, P. J. J. O'Malley, T. C. White, R. Barends, J. Kelly, E. Lucero, M. Mariantoni, A. Megrant,

C. Neill, A. Vainsencher, J. Wenner, A. N. Korotkov, A. N. Cleland, and J. M. Martinis, Phys. Rev. Lett. **110**, 107001 (2013).
[6] J. Wenner, Y. Yin, Y. Chen, R. Barends, B. Chiaro, E. Jeffrey, J. Kelly, A. Megrant, J. Y. Mutus, C. Neill, P. J. J. O'Malley, P. Roushan, D. Sank, A. Vainsencher, T. C. White, A. N. Korotkov, A. N. Cleland, and J. M. Martinis, Phys. Rev. Lett. **112**, 210501 (2014).
[7] F. Helmer, M. Mariantoni, E. Solano, and F. Marquardt, Phys. Rev. A **79**, 052115 (2009).
[8] S. R. Sathyamoorthy, L. Tornberg, A. F. Kockum, B. Q. Baragiola, J. Combes, C. M. Wilson, T. M. Stace, and G. Johansson, Phys. Rev. Lett. **112**, 093601 (2014).
[9] B. Fan, G. Johansson, J. Combes, G. J. Milburn, and T. M. Stace, Phys. Rev. B **90**, 035132 (2014).
[10] K. Zhang, F. Bariani, Y. Dong, W. Zhang, and P. Meystre, Phys. Rev. Lett. **114**, 113601 (2015).
[11] S. Barzanjeh, M. C. de Oliveira, and S. Pirandola, arXiv:1410.4024.
[12] K. Koshino, Phys. Rev. A **79**, 013804 (2009).
[13] K. Koshino, S. Ishizaka, and Y. Nakamura, Phys. Rev. A **82**, 010301(R) (2010).
[14] K. Koshino, K. Inomata, T. Yamamoto, and Y. Nakamura, Phys. Rev. Lett. **111**, 153601 (2013).
[15] K. Inomata, K. Koshino, Z. R. Lin, W. D. Oliver, J. S. Tsai, Y. Nakamura, and T. Yamamoto, Phys. Rev. Lett. **113**, 063604 (2014).
[16] I. Shomroni, S. Rosenblum, Y. Lovsky, O. Bechler, G. Guendelman, and B. Dayan, Science **345**, 903 (2014).
[17] Y.-F. Chen, D. Hover, S. Sendelbach, L. Maurer, S. T. Merkel, E. J. Pritchett, F. K. Wilhelm, and R. McDermott, Phys. Rev. Lett. **107**, 217401 (2011).
[18] B. Peropadre, G. Romero, G. Johansson, C. M. Wilson, E. Solano, and J. J. García-Ripoll, Phys. Rev. A **84**, 063834 (2011).
[19] A. Poudel, R. McDermott, and M. G. Vavilov, Phys. Rev. B **86**, 174506 (2012).
[20] K. Koshino, K. Inomata, Z. Lin, Y. Nakamura, and T. Yamamoto, Phys. Rev. A **91**, 043805 (2015).
[21] R. Vijay, D. H. Slichter, and I. Siddiqi, Phys. Rev. Lett. **106**, 110502 (2011).
[22] M. Hatridge, S. Shankar, M. Mirrahimi, F. Schackert, K. Geerlings, T. Brecht, K. M. Sliwa, B. Abdo, L. Frunzio, S. M. Girvin, R. J. Schoelkopf, and M. H. Devoret, Science **339**, 178 (2013).
[23] Z. R. Lin, K. Inomata, W. D. Oliver, K. Koshino, Y. Nakamura, J. S. Tsai, and T. Yamamoto, Appl. Phys. Lett. **103**, 132602 (2013).
[24] B. Abdo, K. Sliwa, S. Shankar, M. Hatridge, L. Frunzio, R. Schoelkopf, and M. Devoret, Phys. Rev. Lett. **112**, 167701 (2014).
[25] A. Blais, R.-S. Huang, A. Wallraff, S. M. Girvin, and R. J. Schoelkopf, Phys. Rev. A **69**, 062320 (2004).
[26] J. Gambetta, A. Blais, M. Boissonneault, A. A. Houck, D. I. Schuster, and S. M. Girvin, Phys. Rev. A **77**, 012112 (2008).
[27] J. Bylander, S. Gustavsson, F. Yan, F. Yoshihara, K. Harrabi, G. Fitch, D. G. Cory, Y. Nakamura, J.-S. Tsai, and W. D. Oliver, Nat. Phys. **7**, 565 (2011).
[28] C. Rigetti, J. M. Gambetta, S. Poletto, B. L. T. Plourde, J. M. Chow, A. D. Corcoles, J. A. Smolin, S. T. Merkel, J. R. Rozen, G. A. Keefe, M. B. Rothwell, M. B. Ketchen, and M. Steffen, Phys. Rev. B **86**, 100506(R) (2012).
[29] J. Gambetta, W. A. Braff, A. Wallraff, S. M. Girvin, and R. J. Schoelkopf, Phys. Rev. A **76**, 012325 (2007).
[30] C. M. Caves, Phys. Rev. D **26**, 1817 (1982).
[31] L. S. Schulman, Phys. Rev. A **57**, 1509 (1998).
[32] K. Koshino and A. Shimizu, Phys. Rep. **412**, 191 (2005).
[33] K. Koshino, Phys. Rev. Lett. **98**, 223902 (2007).